easily from a harmonic field analysis or transmission line theory:

$$S_{11} = \frac{Z_1 - 1}{Z_1 + 1} \tag{14}$$

$$S_{12} = \frac{1 + \Gamma_2}{1 + \Gamma_2 e^{-\gamma d}} e^{-2\gamma d}(1 + S_{11}) \tag{15}$$

$$S_{21} = S_{12} \tag{16}$$

$$S_{22} = S_{11} \tag{17}$$

where $\gamma = \sqrt{j\omega\mu(\sqrt{2}\sigma + 2j\omega\epsilon)}$, $Z_c = (2\epsilon_r + (\sqrt{2}\sigma)/j\omega\epsilon_0))^{-1/2}$, $Z_1 = Z_c(1 + Z_c th(\gamma d))/(Z_c + th(\gamma d))$, $\Gamma_2 = (1 - Z_c)/(1 + Z_c)$, $\omega = 2\pi f$, $\epsilon = \epsilon_r \epsilon_0$, f is the frequency, ϵ_0 is the permittivity of the vacuum, and ϵ_r, μ, σ, and d are, respectively, the relative permittivity, permeability, and thickness of the conducting shield. And the correction factor 2 and $\sqrt{2}$ is inherent to the slow-wave property of the 2-D TLM network [3].

The transient field that impinges on a plane conducting wall is modeled by the following time function:

$$e_0(t) = Ae^{-t^2/2t_1^2} \tag{18}$$

where A is the value of $e_0(0)$, t is the time, and t_1 is a measure of the pulse width. A plane wave with the above time dependence was incident on the conducting wall (see Fig. 5(a)). The time function was observed at a node located behind the wall after 1000 iterations. The signal is shown in Fig. 5(b) and compared with an analytical approach whose time-domain solution is found by the numerical inverse Fourier transform calculation [10]. Good agreement between two methods can be observed.

V. Conclusion

A novel procedure based on time–frequency transformation for interfacing TLM algorithm with frequency-domain solutions has been presented. It uses the a priori knowledge of the frequency behavior of such parameters as reflection coefficients, network parameters, and impedances, which are known in many practical situations. The relationship between the frequency-domain parameters and the corresponding Johns matrix of the network based on a DFT has been presented in detail. The examples pertaining to modeling of the absorbing waveguide termination and the field penetration through a highly conductive sheet demonstrate the efficiency of the approach. With respect to CPU time, the procedure for generating the Johns matrix pertaining to such problems is orders of magnitude less than that required by other methods.

References

[1] P. B. Johns and R. L. Beurle, "Numerical solution of 2-dimensional scattering problems using a transmission-line matrix," *Proc. Inst. Elec. Eng.*, vol. 118, no. 9, pp. 1203–1208, Sept. 1971.

[2] W. J. R. Hoefer, "The transmission-line matrix method-theory and application," *IEEE Trans. Microwave Theory Tech.*, vol. MTT-33, pp. 882–893, Oct. 1985.

[3] W. J. R. Hoefer, "The transmission line matrix (TLM) method," in *Numerical Techniques for Passive Microwave and Millimeter-Wave Structures*, T. Itoh, Ed. New York: Wiley, 1989, ch. 8, pp. 486–591.

[4] P. So, Eswarappa, and W. J. R. Hoefer, "A two-dimensional TLM microwave field simulator using new concepts and procedures," *IEEE Trans. Microwave Theory Tech.*, vol. 37, pp. 1877–1883, Dec. 1989.

[5] P. B. Johns and S. Akhtarzad, "The use of time domain diakoptics in time discrete models of fields," *Int. J. Numer. Methods Eng.*, vol. 18, pp. 1361–1373, 1982.

[6] Eswarappa and W. J. R. Hoefer, "Application of time domain diakoptics to 3-D TLM method with symmetrical condensed nodes," presented at 1990 IEEE-AP Symp. and URSI Meeting, Dallas, TX, May 7–11, 1990.

[7] W. J. R. Hoefer, "The discrete time domain Green's function or Johns matrix—A new powerful concept in transmission line modelling," *Int. J. Numer. Modelling: Electronic Networks, Devices and Fields*, vol. 2, no. 4, pp. 215–225, 1990.

[8] V. Cizek, *Discrete Fourier Transforms and Their Applications*. Bristol: Hilger, 1986.

[9] Eswarappa, G. I. Costache and W. J. R. Hoefer, "TLM modelling of dispersive wideband absorbing boundaries with time domain diakoptics for *S*-parameters extraction," *IEEE Trans. Microwave Theory Tech.*, vol. 38, Apr. 1990.

[10] C. W. Harrison, Jr., "Transient electromagnetic field propagation through infinite sheets, into spherical shells, and into hollow cylinders," *IEEE Trans. Antennas Propagat.*, vol. AP-12, pp. 319–334, May 1964.

Open Resonator for Precision Dielectric Measurements in the 100 GHz Band

B. Komiyama, M. Kiyokawa, and T. Matsui

Abstract—**Dielectric properties of fused silica, MgO, AlN, and BN were measured using an open resonator at frequencies around 100 GHz. The resonator is of the semiconfocal type and consists of a concave and a plane mirror, and the frequency variation method is used. To increase the reliability of measurement data, the operating frequency and thickness of the samples were chosen so as to make the parameter $\Delta = 1$ for every sample. The radius of curvature of the concave mirror is deduced with sufficient accuracy from the resonant frequencies of the $TEM_{0,0}$ and $TEM_{1,0}$ modes, which results in a precise determination of resonator length. The standard deviation of measurements was less than 0.1% in permittivity and about 10% in loss tangent.**

I. Introduction

Low-loss dielectric materials are of key importance in short-millimeter-wave circuit components and quasi-optical elements such as windows, lenses, beam splitters, and substrates. With increasing demands for improved performance in these components and elements, the measurement of the properties of dielectric materials in this wave band has become more important [1].

In the short-millimeter-wave region, dispersive Fourier transform spectrometers and interferometric spectrometers of the Mach–Zender type are often used for dielectric measurement [1]–[3]. In comparison with these spectrometers, the Fabry–Perot open resonator technique [4] is more advantageous for the measurement of low-loss materials. However, few data were available at frequencies higher than 35 GHz [5], [6] because of the difficulty in constructing high-Q cavities and detecting absorption with enough S/N at these frequencies.

Manuscript received January 7, 1991; revised April 29, 1991. This work was supported by the Science and Technology Agency.

The authors are with the Communications Research Laboratory, 4-2-1 Nukui-Kita Koganei, Tokyo 184, Japan.

IEEE Log Number 9102331.

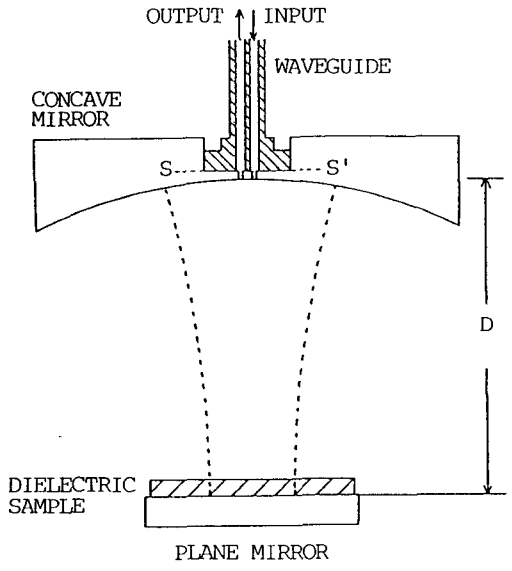

Fig. 1. Schematic diagrams of the semiconfocal open resonator used for dielectric measurement.

In this paper, we describe an open resonator operating at 100 GHz together with measurement results for fused silica, MgO, AlN, and BN. The error of permittivity measurements arising from the measurement resolution in resonator length is discussed in detail.

II. Measurement Method

The open resonator used is of the semiconfocal type, as shown in Fig. 1. The resonator consists of a plane mirror and a concave mirror. The measurement method is well established [4], [7]. We have used the frequency-variation method [4] and Lynch's modified equations [8] as follows.

First, we measure the resonant frequency f_q of a fundamental $TEM_{0,0,q}$ mode of the empty resonator with an arbitrary mode number, q, and calculate the resonator length, D, from the following formula:

$$f_q = \frac{c}{2D}\left[q+1+\frac{1}{\pi}\tan^{-1}\left(\frac{D}{R_0-D}\right)^{1/2}\right] \tag{1}$$

where c is the velocity of light and R_0 is the radius of curvature of the concave mirror. We have used 2.99697×10^8 m/s as a value for c [7]. R_0 is assumed to be accurately known.

The next step is to place a sample with thickness t on the plane mirror and to measure the new resonant frequency, f_s, of the $TEM_{0,0,s}$ mode with the sample present. The permittivity, ϵ_r, or the refractive index, $n=\sqrt{\epsilon_r}$, can be determined by solving the following equation:

$$(1/n)\tan(nkt-\Phi_t) = -\tan(kd-\Phi_d). \tag{2}$$

Here

$$k = 2\pi f_s/c$$

$$d = D - t$$

$$\Phi_t = \tan^{-1}(t/nz_0)$$

$$\Phi_d = \tan^{-1}(d'/z_0) - \tan^{-1}(t/nz_0)$$

where

$$d' = d + t/n$$

$$z_0 = [d'(R_0-d')]^{1/2}.$$

The dielectric loss angle, δ, is given by

$$\tan\delta = \frac{1}{Q_e}\frac{t\Delta+d}{t\Delta+\frac{1}{2k}[\sin 2(kd-\Phi_d)]} \tag{3}$$

where

$$\Delta = \epsilon_r/\{\epsilon_r\cos^2(nkt-\Phi_t)+\sin^2(nkt-\Phi_t)\} \tag{4}$$

and

$$1/Q_e = (1/Q_d)-(1/Q_1).$$

Q_d is the measured Q value of the resonator containing the sample, and Q_1 is the calculated Q value for the resonator containing a similar but loss-free sample. Q_1 is given by

$$Q_1 = Q_0\frac{2(t\Delta+d)}{D(\Delta+1)} \tag{5}$$

where Q_0 is the measured Q value of the empty resonator with the same axial mode number s.

In order to make the most reliable measurements of ϵ_r and δ, a combination of frequency and thickness so as to make $\Delta=1$ is desired [4], [7].

III. Open Resonator and Measurement System

Both the concave mirror and the plane mirror were machined from brass and gold-plated after polishing. The open resonator was designed to measure disk-shaped samples with a diameter of 50 mm. The diameter and the radius of curvature of the concave mirror are 100 mm and 200 mm respectively and the diameter of the plane mirror is 50 mm.

Coupling of microwave power into and out of the resonator is done via two 1-mm-diameter holes with a 2.3 mm center-to-center separation situated symmetrically about the center of the concave mirror [9]. The flange connected to both the input and output WR-10 waveguides is butted against the $S-S'$ face in the back of the concave mirror, as shown in Fig. 1. In order to prevent undesirable direct coupling from one waveguide to the other, 0.2-mm-thick indium seals are used.

Both mirrors are mounted on an aluminum optical rail and arranged so that the axis of the resonator is vertical, as shown in Fig. 1. The plane mirror is mounted on a translation stage and is movable in the direction of the resonator axis.

In order to obtain the optimum coupling coefficients, Q values and insertion losses were measured by varying the length of the coupling holes in steps of about 0.2 mm from an initial length of 1.5 mm, that is, by machining down the $S-S'$ face gradually for the same concave mirror.

The measurement results are shown in Fig. 2, where the resonator is operated with the fundamental $TEM_{0,0}$ mode, $D=107$ mm, and the resonant frequency is 101.3 GHz. The solid line of Fig. 2 is the calculated value of the insertion loss under the assumption that the coupling coefficients of the two holes are equal [10]. The absolute value of calculation is chosen to coincide with the measured value at a length of 1.5 mm. Good agreement between calculation and experiment is obtained. With the length of the coupling holes now being 1.05 mm in our experiments, the insertion loss is about 25 dB, which

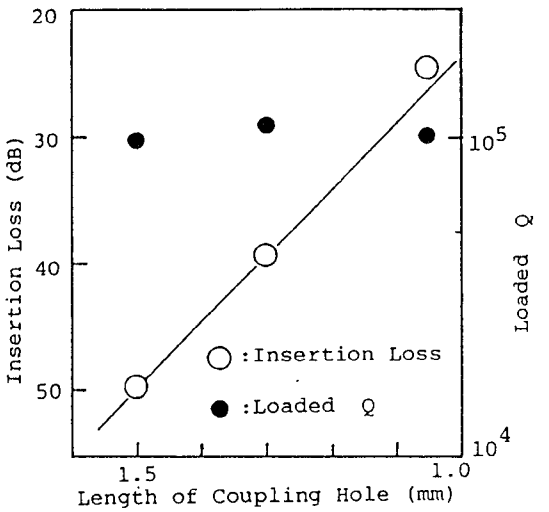

Fig. 2. Insertion loss and loaded Q versus length of coupling hole.

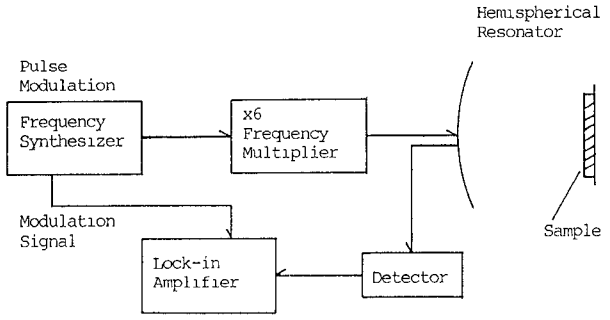

Fig. 3. Block diagram of measurement system.

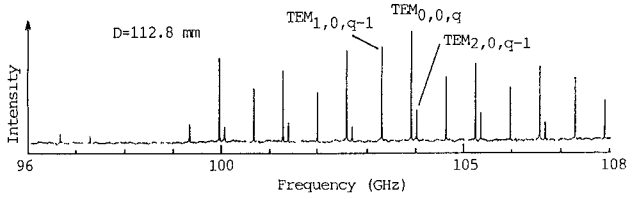

Fig. 4. Mode spectrum of the open resonator with $D = 112.8$ mm.

is satisfactory for our measurements. The Q value is almost constant for a variation of the coupling hole length from 1.5 mm to 1.05 mm and is 1.1×10^5.

A block diagram of measurement system is shown in Fig. 3. A frequency multiplier driven by a pulse-modulated synthesizer is fed to the resonator, and the transmission signal from the resonator is detected by a square-law detector and a lock-in amplifier. The frequency multiplier (the multiplication factor is 6) covers the entire W band and its nominal output power is 0 dBm. Q values are determined by the slope of the plots of reduced cavity parameters versus reduced frequency parameters [11].

An example of the mode spectrum of the resonator with $D = 112.8$ mm is shown in Fig. 4 when sweeping frequencies from 96 to 108 GHz. In addition to the fundamental mode, $TEM_{1,0}$ and $TEM_{2,0}$ modes are excited. The Q value of the $TEM_{1,0}$ mode is almost as high as that of the $TEM_{0,0}$ mode. Although the resonant frequency of the $TEM_{2,0}$ mode is close

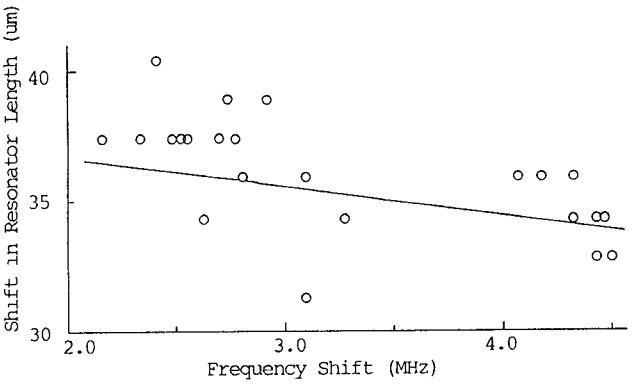

Fig. 5. Plots for D calculated from f_{77} and f_{76} versus f_{77}. Vertical and horizontal axes show shifts from 112.8 mm and 103.944 GHz. respectively. The solid line shows the D calculated by (1) with $R_0 =$ 198.50 mm.

to that of the $TEM_{0,0}$ mode, mode identification is quite easy, because both the Q value and the detected signal level are much lower than those of the $TEM_{0,0}$ mode. The signal intensity becomes very small between 96 and 99.5 GHz. We cannot adequately explain this yet.

IV. Error of ϵ_r Caused by Measurement Resolution in D

The fractional error of permittivity, $\delta\epsilon_r/\epsilon_r$, arising from the measurement error of the resonator length δD can be written by differentiating (2):

$$\delta\epsilon_r/\epsilon_r \doteq -2\delta D/t \tag{6}$$

where it is assumed that D and f_q are independent of each other and that $\Delta = 1$ and $t \ll D$.

In a measurement system such as that of Fig. 3, the fractional frequency measurement resolution, δ_m, is usually of the order of $1/(100Q_0)$. In our case, δ_m is about 3×10^{-7}. From (1), D can be written as

$$D = c/2\left[\left(f_q - f_{q-1}\right)\right]. \tag{7}$$

Hence,

$$\frac{\delta D}{D} = \frac{1}{f_B}\left(f_q^2 + f_{q-1}^2\right)^{1/2}\delta_m \tag{8}$$

where $f_B = c/2D$ and no correlation between measurements of f_q and f_{q-1} is assumed. For our typical case ($D = 113$ mm, $f_q = 100$ GHz), $\delta D/D \sim 3.2 \times 10^{-5}$. Fig. 5 shows the plots for D calculated from f_{77} and f_{76} by using (7) versus f_{77}. Changes in f_{77} are due to a variation of ambient temperature of about 1.6° C. The predicted fluctuation of D is observed. The error in ϵ_r for a sample 1 mm in thickness becomes about 1% in the case above. Therefore, D is determined from (1) to reduce this error [4], [12], as described in Section II. However, this can only be allowed on the assumption that R_0 is measured precisely. Differentiating (1) gives

$$\delta D/D \doteq -(c/4\pi f_q)\left[D(R_0 - D)\right]^{-1/2}(\delta R_0/R_0) \tag{9}$$

where $(c/4\pi f)\left[D(R_0 - D)\right]^{-1/2} \ll 1$ is assumed. For the case above and with $R_0 = 200$ mm, dR_0/R_0 should be less than 1.3×10^{-3} to determine $\delta D/D$ by less than 3.2×10^{-6}.

Jones has determined R_0 by measuring the difference of the resonator lengths between adjacent modes with a resolution of

TABLE I
MEASURED R_0 FOR VARIOUS RESONATOR LENGTHS

D (mm)	R_0 (mm)
110.836	198.493
112.839	198.504
114.837	198.517
mean values: 198.50 ± 0.01 mm	

0.2 μm for a series of q values and fitting calculated values from (1) to the measured results [7]. We have measured R_0 more simply and conveniently by using the resonant frequencies of both the $TEM_{0,0}$ and $TEM_{1,0}$ modes. The resonant frequency, $f_{p,0,q}$, for the $TEM_{p,0,q}$ mode is

$$f_{p,0,q} = \frac{c}{2\pi D}\left\{(q+1)\pi + (2p+1)\tan^{-1}\left(\frac{D}{R_0 - D}\right)^{1/2}\right\}. \quad (10)$$

From (10), R_0 and the fractional error of R_0 can be written as follows by using $f_{0,0,q}$, $f_{1,0,q-1}$, and $f_{0,0,q-1}$:

$$R_0 = D\sin^{-2}(\pi x/2) \quad (11)$$

$$dR_0/R_0 = \alpha\delta_m \quad (12)$$

where

$$x = f_{B2}/f_{B1}$$

$$\alpha = \pi x\beta\cot(\pi x/2)$$

$$\beta = \left[\left(f_{1,0,q-1}/f_{B2}\right)^2 + \left(f_{0,0,q}/f_{B1}\right)^2 + \left(f_{B1}^{-1} - f_{B2}^{-1}\right)^2\left(f_{0,0,q-1}\right)^2\right]^{1/2}$$

$$f_{B1} = f_{0,0,q} - f_{0,0,q-1}$$

$$f_{B2} = f_{1,0,q-1} - f_{0,0,q-1}.$$

In the derivation of (12), we have assumed that the measurement resolution of $f_{0,0,q}$, $f_{0,0,q-1}$, and $f_{1,0,q-1}$ is the same and measurements of these frequencies have no correlation each other.

Since $x \sim 1/2$ in our case, as shown in Fig. 4, we can show that dR_0/R_0 is nearly equal to the fractional error of D given by (8) and is sufficiently small for our purpose.

Table I shows measured results by this method for three different values of D, which are within ± 10 μm. The solid line in Fig. 5 is the D calculated by (1) with $R_0 = 198.50$ mm, which also demonstrates the suitability of this method.

The obtained R_0 differs from the mechanically assigned value of 200 mm by as much as 1.5 mm. The reason for this large discrepancy is under investigation.

Although R_0 can be measured with sufficient accuracy by this method, its use is limited to the case where the $TEM_{1,0}$ mode with a Q similar to the fundamental mode exists. When the $TEM_{1,0}$ mode is not available, it will be necessary to further increase the measurement resolution of the resonant frequency by a technique such as frequency locking a millimeter-wave source to the resonator [13].

V. DIELECTRIC MEASUREMENT

Measurements were made on fused silica, MgO, AlN, and BN. All samples are disk-shaped with diameter of 50 mm and polished faces. The sample is just placed on the plane mirror as shown in Fig. 1 and no clamp is used.

The results are summarized in Table II. The measurement frequency has been chosen to make $\Delta = 1$ for each sample. The double entries in the table refer to the one sample being turned over.

TABLE II
MEASURED PERMITTIVITY AND LOSS TANGENT

Material	t (mm)	f (GHz)	Δ	ϵ_r	$\tan\delta \times 10^4$
Silica Glass	1.46	105.3	1.00	3.799	2.6
				3.800	2.5
	2.94	105.3	1.00	3.800	2.9
				3.800	3.0
IR grade	5.12	104.7	1.00	3.800	3.1
				3.800	3.3
MgO	1.04	92.8	1.00	9.809	0.42
				9.813	0.49
AlN	1.12	92.9	1.00	8.289	4.6
				8.290	4.5
	2.18	96.5	1.01	8.296	3.8
				8.297	4.1
BN	1.93	103.0	1.00	5.163	11
				5.163	10

We have measured three samples with different thicknesses of fused silica to check for systematic error. The samples are IR grade fused silica from the Nippon Silica Glass Company and the OH content is about 8 ppm according to the manufacturer's data sheets. No significant change can be seen in ϵ_r up to the third figure among the three samples. Measured values of ϵ_r are about 0.2% smaller than those of fused silica with low water content measured at 245 GHz [2]. For $\tan\delta$, there is a tendency for a thicker sample to show a higher $\tan\delta$.

MgO is often used as a substrate for high-T_c superconductors [14]. The sample used is a ⟨100⟩ face single crystal and is produced by Tateho Chemical Industry. Our results for ϵ_r and $\tan\delta$ are about 5% higher and 2.5 times larger, respectively, than those measured at 15 GHz [14]. The $\tan\delta$ of MgO is smaller than that of fused silica by nearly an order of magnitude and is therefore a promising substrate for superconducting microwave devices.

AlN and BN are potential candidates for window materials in high-power source applications such as gyrotrons and klystrons, because of their good thermal conductivity. The AlN sample was obtained from Sumitomo Electric Industry and is 99.7% chemically pure. The average ϵ_r for the AlN samples is 2.1% higher than the value reported in [3].

The BN sample was obtained from DENKA and is designated P-BN. The sample is pylolitic BN; it is prepared by the CVD method, and the total content of metallic impurities according to manufacturer's data sheets is less than 10 ppm. The measured ϵ_r shows a value higher than that reported in [2] for hot-pressed BN. This material is lossier than AlN.

For all samples in Table II, the standard deviation of measurement error is less than 0.1% in ϵ_r and about 10% in $\tan\delta$.

VI. CONCLUSION

With the recent progress in commercial millimeter-wave wide-band frequency sources, it has been shown that an open resonator can be a convenient tool for precise measurements of permittivity and loss tangent for low-loss material even at 100 GHz.

Dielectric properties of fused silica, MgO, AlN, and BN at 100 GHz have been measured. Standard deviations in the measurements of less than 0.1% for ϵ_r and of about 10% for $\tan\delta$ have been achieved.

ACKNOWLEDGMENT

The authors would like to thank Dr. T. Shimozuma of the Mitsubishi Electric Corporation for offers of several samples. They would also like to thank their colleague Dr. C. E. Tong for his invaluable discussions.

REFERENCES

[1] M. N. Afsar and K. J. Button, "Millimeter-wave dielectric measurement of materials," *IEEE Trans. Microwave Theory Tech.*, vol. MTT-33, pp. 131–153, Jan. 1985.
[2] J. M. Dutta, C. R. Jones, and H. Dave, "Complex dielectric constants for selected near-millimeter-wave materials at 245 GHz," *IEEE Trans. Microwave Theory Tech.*, vol. MTT-34, pp. 932–936, Sept. 1986.
[3] S. Nakashima *et al.*, "Construction of millimeter- and submillimeter-wave interferometric spectrometer and its application to measurement of optical constants," Oyo Bururi (Japan), vol. 59, pp. 1093–1102, May 1990.
[4] A. L. Cullen, *Infrared and Millimeter Waves*, vol. 10, *Millimeter-Wave Open-Resonator Techniques*, New York: Academic Press, 1983, pp. 233–280.
[5] R. Watanabe and N. Nakajima, "Precise dielectric measurements at 100 GHz range using Fabry-Perot resonator," *Trans. IECE (Japan)*, vol. 61-B, pp. 205–207, Mar. 1978.
[6] M. N. Afsar, T. Matsui, and Hua Chi, "A precision 60 GHz open resonator system for permittivity and loss tangent measurement of low absorbing materials," in *Proc. Conf. Precision Electromagnetic Measurements*, June 1988, pp. 145–146.
[7] R. G. Jones, "Precise dielectric measurements at 35 GHz using an open microwave resonator," *Proc. Inst. Elec. Eng.*, vol. 123, pp. 285–290, Apr. 1976.
[8] A. C. Lynch, "Open resonator for the measurement of permittivity," *Electron. Lett.*, vol. 14, p. 596, Aug. 1978.
[9] J. W. Dees and A. P. Sheppard, "Fabry–Perot interferometers at 168 Gc/s," *IEEE Trans. Instrum. Meas.*, vol. IM-11, pp. 52–58, 1965.
[10] S. B. Cohn, "Microwave coupling by large apertures," *Proc. IRE*, vol. 40, pp. 696–699, June 1952.
[11] K. D. Mckinstry and C. E. Patton, "Methods for determination of microwave cavity quality factors from equivalent electronic circuit models," *Rev. Sci. Instrum.*, vol. 60, pp. 439–443, Mar. 1989.
[12] A. L. Cullen, P. Nagenthiram, and A. D. Williams, "Improvement in open resonator permittivity measurement," *Electron. Lett.*, vol. 8, pp. 577–579, Nov. 1972.
[13] C. Audoin, "Fast cavity auto-tuning system for hydrogen masers," *Rev. Phys. Appl.*, vol. 16, pp. 125–130, Mar. 1981.
[14] A. A Valenzuela and P. Russer, "High Q coplanar transmission line resonator of $YBa_2Cu_3O_{7-x}$ on MgO," *Appl. Phys. Lett.*, vol. 55, pp. 1029–1031, Sept. 1989.
[15] Y. Kobayashi, K. Yajima, and J. Sato, "Low temperature dependence of complex permittivity on MgO and $SrTiO_3$ substrate at microwave frequencies," IEICE Technical Report (Japan), SCE89-1, pp. 1–6, Apr. 1989.

A Method for the Rapidly Convergent Representation of Electromagnetic Fields in a Rectangular Waveguide

Kazuhisa Ishibashi and Eikichi Sawado

Abstract—**In numerically analyzing the electromagnetic fields in a rectangular waveguide by the integral equation method, it is essential to calculate the electromagnetic fields produced by the electric and magnetic currents and charges. In this paper, a new method is proposed to facilitate rapid calculation of the three-dimensional fields. This method is a modified image method and gives an accurate value in a short time.**

Manuscript received January 25, 1991; revised April 30, 1991.

K. Ishibashi is with Corporate Research and Development, Toyo Seikan Group, 22-4 Okazawacho, Hodogayaku, Yokohama, 240 Japan.
E. Sawado is with the Faculty of Engineering, Tokyo Metropolitan University, 2-1-1 Fukazawa, Setagayaku, Tokyo, 158 Japan.

IEEE Log Number 9102328.

I. INTRODUCTION

The integral equation method has been effectively used to analyze electromagnetic fields in a rectangular waveguide [1]–[3]. In solving integral equations, it is desirable to calculate the fields produced by electromagnetic sources, such as electric and magnetic currents and charges, within a short time.

The fields have usually been expressed by the mode method or the image method [4]. In the mode method, the field is expressed by a series using modal functions which satisfy the boundary conditions on the waveguide wall (here called the mode series). In the image method, the field is expressed by a series which is composed of fields produced by a source and its images arranged to infinity in order to satisfy the boundary conditions on the waveguide wall (here called the image series). As the fields are expressed by infinite series, the convergence of the series is sometimes troublesome and several methods have been proposed for rapid computation. There is a rapid convergence method [1], [2] for two-dimensional fields and a modified image method [3] for three-dimensional fields.

A modified image method for calculating the fields produced by straight electric and magnetic current segments has been proposed and found to be effective for calculating the fields near the source. Computing errors of the fields increase as the distance from the source to the observation point increases. Therefore, the modified image method is improved for the accurate calculation at any position by adding a correcting term. In order to check the adequacy and usefulness of the method considering the term, its error is compared with that of the method without it.

II. REPRESENTATIONS OF THE ELECTROMAGNETIC FIELDS

The electric and magnetic fields, $\boldsymbol{E}$ and $\boldsymbol{H}$, in the Lorentz gauge are expressed by using the vector potentials $\boldsymbol{A}$ and $\boldsymbol{A}^*$ produced respectively by electric and magnetic currents $\boldsymbol{i}$ and $\boldsymbol{i}^*$ and the scalar potentials ϕ and ϕ^* produced respectively by electric and magnetic charges ρ and ρ^* as follows [5]:

$$\boldsymbol{E} = -j\omega\boldsymbol{A} - \nabla\phi - \nabla\times\boldsymbol{A}^*/\epsilon_0 \tag{1}$$

$$\boldsymbol{H} = -j\omega\boldsymbol{A}^* - \nabla\phi^* + \nabla\times\boldsymbol{A}/\mu_0 \tag{2}$$

where ϵ_0 and μ_0 are, respectively, the permittivity and the permeability and $\omega = 2\pi f$ with a frequency f.

Setting the Cartesian coordinates with the z axis parallel to the direction of wave propagation and the x and y axes parallel to each wall of the waveguide, we obtain the vector and scalar potentials at $P_0(x_0, y_0, z_0)$ produced by the currents and charges positioned at $P_s(x_s, y_s, z_s)$.

A. Representation of the Fields by the Image Method

The potentials are given equivalently by adding those produced by electromagnetic sources such as $\boldsymbol{i}$, $\boldsymbol{i}^*$, ρ, and ρ^* and their images $\boldsymbol{i}_t$, $\boldsymbol{i}_t^*$, ρ_t, and ρ_t^* [3].

The images are positioned at $P_t(x_t, y_t, z_t)$:

$$x_t = 2am + (-1)^k x_s \qquad y_t = 2bn + (-1)^l y_s \qquad z_t = z_s$$